MC3D: simulating polarization maps and more

Sebastian Wolf, Thomas Henning, Bringfried Stecklum

Sebastian Wolf, Thomas Henning, Bringfried Stecklum, "MC3D: simulating polarization maps and more," Proc. SPIE 4843, Polarimetry in Astronomy, (14 February 2003); doi: 10.1117/12.458867

SPIE.

Event: Astronomical Telescopes and Instrumentation, 2002, Waikoloa, Hawai'i, United States

MC3D - Simulating Polarization Maps and more!

S. Wolf[a], Th. Henning[b], and B. Stecklum[c]

[a]California Institute of Technology, 1200 E California Blvd, Pasadena, CA 91125, USA
[b]Max-Planck-Institut für Astronomie, Königsstuhl 17, 69117 Heidelberg, Germany
[c]Thüringer Landessternwarte Tautenburg, Sternwarte 5, 07778 Tautenburg, Germany

ABSTRACT

MC3D is a three-dimensional, self-consistent continuum radiative transfer code. It can be used to determine the spatial temperature distribution in arbitrary dust/electron configurations, such as around young stellar objects or active galactic nuclei. Based on this temperature distribution, MC3D allows calculation of polarization maps, images, and spectral energy distributions. We present the numerical techniques applied in this code, describe its capabilities, and show instructive examples of previous applications.

Keywords: Radiative transfer, Monte-Carlo method, Polarization

1. INTRODUCTION

The 3D continuum radiative transfer (RT) code MC3D combines the most recent Monte Carlo (MC) radiative transfer concepts for both the self-consistent RT, i.e., the estimation of spatial dust temperature distributions, and pure scattering applications, taking into account the polarization state of the radiation field. It has been tested intensively and compared with grid-based and other MC RT codes.[1,2]

Previous applications of MC3D cover feasibility studies of extrasolar planet detections,[3] the RT in the clumpy circumstellar environment of young stellar objects,[4] polarization studies of T Tauri stars,[5] AGN polarization models,[6] a solution for the multiple scattering of polarized radiation by non-spherical grains,[7] and the inverse RT based on the MC method.[8]

The executables of MC3D can be downloaded for several model geometries and computer platforms from `http://www.mpia-hd.mpg.de/FRINGE/SOFTWARE/mc3d/` (current US mirror page: `http://spider.ipac.caltech.edu/staff/swolf/mc3d/`). Furthermore, usage instructions and IDL* routines for a subsequent data analysis of the code are provided there. Very frequently used model geometries, such as disks with a radial and vertical variable density distribution, which are often used for the analysis of SEDs, images and polarization maps of circumstellar disks,[9–11] are available. A detailed description of MC3D has been published by Wolf et al.[12] and Wolf.[13]

2. GENERAL OVERVIEW

2.1. Three-dimensional Monte-Carlo radiative transfer

Each model to be considered with MC3D consists of two independently defined components:

1. The spatial density distribution of the scattering and absorbing medium, and
2. The radiative source(s).

Further author information: (Send correspondence to S. Wolf)
S. Wolf: E-mail: swolf@ipac.caltech.edu, Telephone: 1 626 395 8794
*Interactive Data Language

Polarimetry in Astronomy, Silvano Fineschi, Editor, Proceedings of SPIE
Vol. 4843 (2003) © 2003 SPIE · 0277-786X/03/$15.00

Both must be defined inside a convex model space in order to exclude the case of radiation leaving the model space at one point and entering it at another.

MC3D handles spherically symmetric scatterers/absorbers, such as spherical dust grains and electrons (in the Thomson scattering regime) but spheroidal grains as well. It allows simulation of the RT in arbitrary density distributions, $\rho_j(\vec{r})$, where $\vec{r}$ represents the spatial coordinate and the index j refers to the considered dust species (characterized by the grain size and chemical composition). The density distributions may be defined either analytically or on a predefined grid in order to allow the implementation of density distributions resulting from hydrodynamical simulations (for examples, see Wolf et al.,[14] Sect. 4; Wolf et al.[3]).

Radiation sources, that are arbitrary with respect to their number and spatial configuration, spatial extent, intrinsic SED, and radiation characteristic can be considered (see Wolf et al.[3, 14] for examples). In MC3D the RT is simulated at certain wavelengths within a given wavelength range. For this reason, the luminosity of the radiation source(s) is partitioned into n_{Photon} so-called "weighted photons" each of which is characterized by its wavelength λ and Stokes vector $\hat{I} = (I, Q, U, V)^{\mathrm{T}}$.

The mean free path length l between the point of emission and the point of the first photon-dust interaction (and - subsequently - between two points of interaction) is given by

$$\tau_{\mathrm{ext,l}} = -\ln(1 - Z), \tag{1}$$

$$\tilde{\tau}_{\mathrm{ext,l}} = \sum_{i=1}^{i_{\mathrm{end}}} \left[\sum_{j=1}^{n_{\mathrm{D}}} \rho_j(\vec{r}_{\mathrm{l_i}}) \cdot C_{\mathrm{ext_j}} \right] \cdot \Delta l_i, \qquad l = \sum_{i=1}^{i_{\mathrm{end}}} \Delta l_i. \tag{2}$$

Here, n_{D} is the number of different dust grain species, $\tau_{\mathrm{ext,l}}$ is the optical depth along the geometrical path l, $\vec{r}_{\mathrm{l_i}}$ is the spatial coordinate corresponding to the ith integration point along the path length l, $C_{\mathrm{ext_j}}$ is the extinction cross section of the jth dust species, and Z is a random number uniformly distributed in the interval $[0, 1]$.

This photon transfer concept was found to limit the applicability of the previous version of MC3D to optical depths $\tau \geq 10^{-3}$ since the probability for photons to interact with the (circumstellar) matter is negligibly small for even lower optical depths[12] (it decreases exponentially as described by Bouguer-Lambert's law). In order to consider lower optical depths, for instance the simulation of the scattered light arising from an optically thin envelope or the electron environment around hot stars, the concept of enforced scattering[15] has been implemented. The idea is to force each photon to be scattered at least once between the point of emission and the boundary of the model space, provided there is dust on its path.

2.2. Estimation of the spatial dust temperature distribution

Two different concepts for the solution of the self-consistent RT problem, i.e., the determination of the spatial dust temperature distribution on the basis of the amount of absorbed energy of the stellar and the dust reemission radiation field, are embedded in MC3D.

The first concept is based on an iterative procedure:

1. Heating by the star.
2. Reemission by the dust grains, based on the energy being absorbed from the stellar radiation field.
3. Reemission of the dust grains, based on the sum of the energy being absorbed from the stellar and the dust reemission radiation field.

Here, the third step has to be repeated as long as the difference between the input energy (given by the stellar radiation field) and the output energy (given by the sum of the attenuated stellar radiation field and the reemitted radiation outside the model space) is larger than a user-specific treshold (e.g., 0.1% of the input energy).

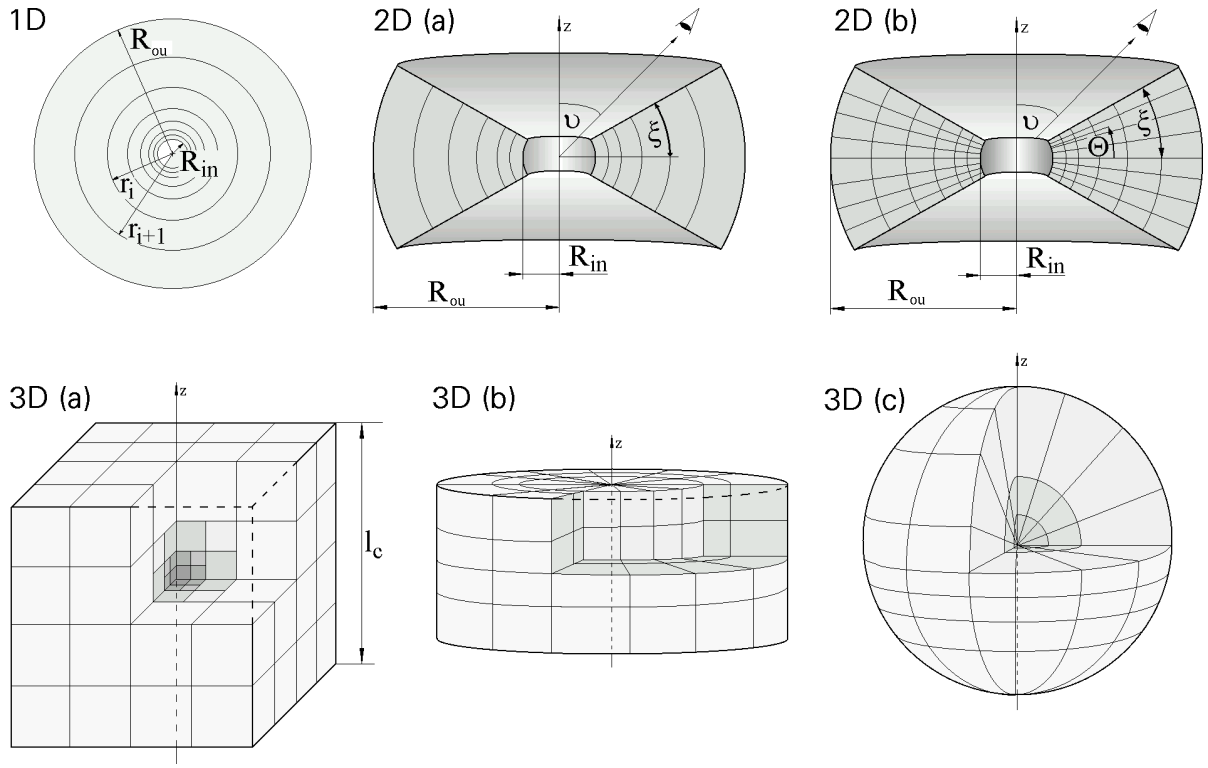

Figure 1. Model geometries: Examples for the subdivision of the model space into energy storage cells (see Sect. 2.2 for further explanations). **1D:** radial symmetry; **2D(a):** radial symmetry inside a disk; **2D(b):** fully two-dimensional model for configurations with a radial and vertical dependence of the density distribution; **3D(a-c):** three-dimensional models considered in cartesian, cylindrical, and spherical coordinates. *(taken from Wolf 2002*[13]*)*

The second concept embedded in MC3D for the estimation of the spatial dust temperature distribution has recently been advised by Bjorkman & Wood.[16] It is based on the immediate determination of the increased dust temperature due to the absorption of each single photon. To correct the temperature of the considered dust grain, the wavelength of the immediately reemitted photon is chosen so that it corrects the temperature of the spectrum previously emitted by this particular grain, i.e., the probability distribution of the reemission wavelength is given by

$$f(\lambda) \propto Q_{\rm abs}\ [B_\lambda(\bar{T}_{\rm g_j}(i)) - B_\lambda(\bar{T}_{\rm g_j}(i-1))], \tag{3}$$

where $\bar{T}_{\rm g_j}(i-1)$ represents the temperature of the grain species j before and $\bar{T}_{\rm g_j}(i)$ after the ith absorption process.

To reduce the number of photons being required for the temperature estimation in optically thin configurations, the concept of Lucy[17] is applied. It considers the absorption of the electromagnetic radiation field not only at the end points of the photon path (points of interaction) but also in between.

To achieve a spatially resolved dust temperature distribution, the model space is subdivided into so-called energy storage cells in which the absorbed energy of the radiation field is accumulated and in which a constant dust temperature is assumed. To represent the spatial temperature structure according to the model geometry, defined by both the spatial distribution of radiation sources and the dust density, the model space has to be subdivided taking this into account. The geometries considered in MC3D are illustrated in Fig. 1.

2.3. Observables

Polarization maps, images, and SEDs can be directly simulated with MC3D. In order to derive these observables, a photon will be recorded in an observing plane oriented perpendicular to the path of the photon as soon as its

next scattering position would be located outside the model space.

Spatially resolved images (such as shown in Fig. 2, 3, 4, and 5) are obtained by subdividing the observing planes into pixels. Regarding the last scattering position of a photon, its (projected) Stokes parameters, wavelength and monochromatic luminosity are stored in the corresponding pixel. The required transformation of the Stokes vector was outlined by Fischer.[18] Furthermore, MC3D is equipped with a raytracer being optimized for the 1D and 2D models shown in Fig. 1. It allows derivation of images and the SED resulting from the dust reemission radiation. It is based on the assumption that scattering processes are negligible in the corresponding mid-infrared to millimeter wavelength range which is very well fulfilled for most of the astrophysical applications targeted by MC3D.

3. SIMULATION OF LINEAR AND CIRCULAR POLARIZATION

The polarization state of a photon is determined by the Stokes vector components as follows:

$$\begin{array}{lcl} \text{(a) Linear polarization degree} & : & P_{\rm l} = \frac{\sqrt{(Q^2+U^2)}}{I} \\ \text{(b) Orientation of the linear polarization} & : & \gamma = \frac{1}{2}\arctan\left(\frac{U}{Q}\right) \\ \text{(c) Circular polarization degree} & : & P_{\rm c} = \frac{V}{I}\ . \end{array} \tag{4}$$

3.1. Spherical grains / Electrons

The scattering matrix (special Müller matrix) for the description of the modification of the Stokes vector due to the interaction of a weighted photon with a spherical, homogeneous dust particle has the form

$$\hat{S}(\theta) = \begin{pmatrix} S_{11}(\theta) & S_{12}(\theta) & 0 & 0 \\ S_{12}(\theta) & S_{11}(\theta) & 0 & 0 \\ 0 & 0 & S_{33}(\theta) & S_{34}(\theta) \\ 0 & 0 & -S_{34}(\theta) & S_{33}(\theta) \end{pmatrix}, \tag{5}$$

where

$$\begin{array}{l} S_{11}(\theta) = \frac{1}{2}(|S_1(\theta)|^2 + |S_2(\theta)|^2 + |S_3(\theta)|^2 + |S_4(\theta)|^2) \\ S_{12}(\theta) = \frac{1}{2}(|S_2(\theta)|^2 - |S_1(\theta)|^2 + |S_4(\theta)|^2 - |S_3(\theta)|^2) \\ S_{33}(\theta) = \mathrm{Re}\{S_1(\theta)S_2^*(\theta) + S_3(\theta)S_4^*(\theta)\} \\ S_{34}(\theta) = \mathrm{Re}\{S_2(\theta)S_1^*(\theta) + S_4(\theta)S_3^*(\theta)\}\ . \end{array} \tag{6}$$

Here, the quantities $S_{1\ldots4}$ are the wavelength-dependent scattering amplitudes which are given by Mie theory and the quantity θ is the scattering angle.

The first example for the solution of the radiative transfer problem under consideration of polarization due to light scattering by spherical dust grains is illustrated in Fig. 2. K band polarization maps for a model of a low-mass YSO being surrounded by a circumstellar disk are shown. The spatial density structure and initial temperature distribution of the circumstellar disk ($M = 2.3 \times 10^{-3}\,M_{\rm sun}$) results from hydrodynamical simulations performed by Yorke (1999, priv. comm.).

In the second example, the influence of a large-scale clumpy structure in the circumstellar dust shell around a young stellar object on the resulting polarization pattern is investigated. The clumps are represented by two optically thick small spheres (2,3) embedded in an optically thin large sphere (1, circumstellar envelope). The disturbance of the centro-symmetric dust distributions results in a disturbance of the centro-symmetric polarization pattern. Whereas both clumps are visible in the intensity map (Fig. 3(B)), the effect of the deeper embedded clump on the polarization pattern can be neglected (Fig. 3(C)).

In case of Thomson scattering, the scattering matrix elements are wavelength-independent and can be written as

$$\begin{array}{l} S_{11}(\theta) = S_{22}(\theta) = (\cos^2(\theta) + 1)/2 \\ S_{12}(\theta) = S_{21}(\theta) = (\cos^2(\theta) - 1)/2 \\ S_{33}(\theta) = S_{44}(\theta) = \cos(\theta) \\ S_{13} = S_{31} = S_{23} = S_{32} = 0 \\ S_{14} = S_{24} = S_{34} = S_{43} = 0 \end{array} \tag{7}$$

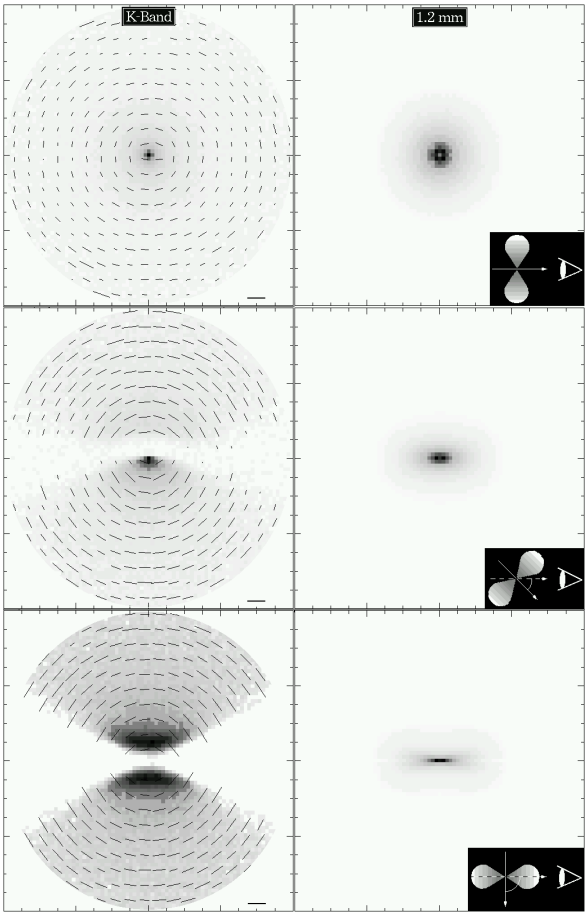

Figure 2. Intensity maps with overlaied polarization pattern of a young stellar object configuration consisting of a circumstellar disk and an optically thin circumstellar envelope. The configuration is shown for inclination of υ=0° (face-on), 45°, and 90° at the wavelengths λ=2.2μm (K band, left column) and 1.2 mm (right column). The scale in the lower right edge of the images correspond to a polarization degree of 100 %. *(taken from Wolf 2001[2])*

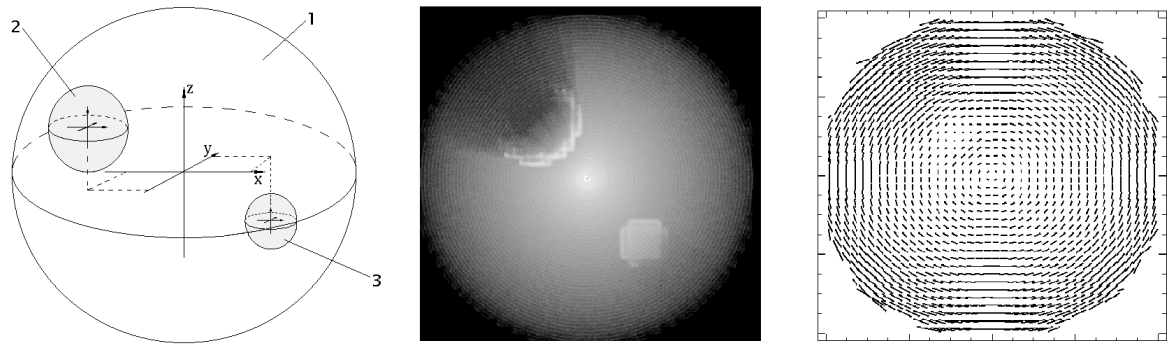

Figure 3. A: Example for the influence of large spherical, optical thick clumps embedded in an optically thin medium on the polarization pattern of the shell. **B**: Intensity map of the dust configuration shown in Fig. 3(A). The observer looks along the positive y-axes. **C**: Polarization map of the dust configuration shown in Fig. 3(A). The observer looks towards the y-axes. *(taken from Wolf et al. 1998[4])*

(see Bohren & Huffman[19]). A typical application for the combination of light scattering both by dust grains and electrons is the simulation of the radiative transfer in active galactic nuclei.[6]

3.2. Spheroidal grains

Even in the case of simply-structured objects like ordinary reflection nebulae, deviations of polarization vectors from the direction perpendicular to the illuminating star were discovered more than three decades ago.[20] These deviations may be explained by light scattering on non-spherical grains aligned by a magnetic field. Non-centrosymmetric polarization patterns have been observed in bipolar and cometary nebulae and young stellar objects,[21] evolved stars,[22] and are also clearly seen in polarization maps of comets.[23] They may be attributed to non-spherical grains, although they could be caused by multiple scattering on spherical particles as well. Another effect which may be related to the light scattering by non-spherical grains is the wavelength dependence of the positional angle of polarization observed in red giants, AGB stars, and bipolar reflection nebulae.[24] Furthermore, very high degrees of circular polarization of scattered light in the Orion molecular cloud were measured.[25] It is assumed that the circular polarization is produced by aligned non-spherical grains because multiple scattering of radiation by spherical or randomly oriented non-spherical grains results in a much smaller circular polarization degree than observed. In addition, the interstellar polarization and polarized thermal emission phenomena prove that non-spherical grains exist in the interstellar medium. These effects arise because of dichroic extinction/emission of radiation by aligned non-spherical grains and were modeled with spheroidal grains.[26–28]

The main features distinguishing the light scattering by aligned non-spherical particles and spherical particles are:

1. Azimuthal dependence of the scattered radiation;
2. Linear polarization in the forward and backward directions;
3. Deviation of the positional angle of linear polarization after first scattering from the direction perpendicular to the illuminating source and
4. Circular polarization after first scattering.

These features result from the fact that in the general case of non-spherical particles — in contrast to spherical grains (see Eq. 5) — all 16 elements of the scattering matrix are non-zero.[29]

For illustration of the differences resulting from light scattering in an environment containing aligned spheroidal instead of spherical grains, in Fig. 4 intensity maps with overlaied polarization pattern of a spherical shell containing perfectly aligned dust grains are shown. In the case of nearly spherical grains (axis ratio $a/b = 1.1$), the ring-like structure which results from light scattering at the inner boundary of the circumstellar shell is clearly seen for oblate as well as for prolate grains. Otherwise, in the case of $a/b = 2$ the intensity maxima appear at the points of intersection with the z (perpendicular to the z)-axis for oblate (prolate) grains. In both cases, the corresponding axis is parallel to the minor (b) axis of grains. Increasing the aspect ratio a/b, this effect is strengthened.

In Fig. 5, the circular polarization resulting from light scattering by aligned oblate dust grains in a geometrically and optically thin dust shell is shown. The circular polarization is equal to zero in the midplane and along the line through the centre perpendicular to the midplane. The net circular polarization from the configuration is also equal to zero.

3.3. Conclusions

We described the publically available[12, 13] computer program MC3D for self-consistent 3D continuum radiative transfer calculations. Based on an efficient implementation of the Monte-Carlo method, it allows simulation of the spatial temperature distributions of arbitrary dust density configurations with embedded stars or similar energy sources. Subsequently polarization maps, spectral energy distributions, and images can be derived.

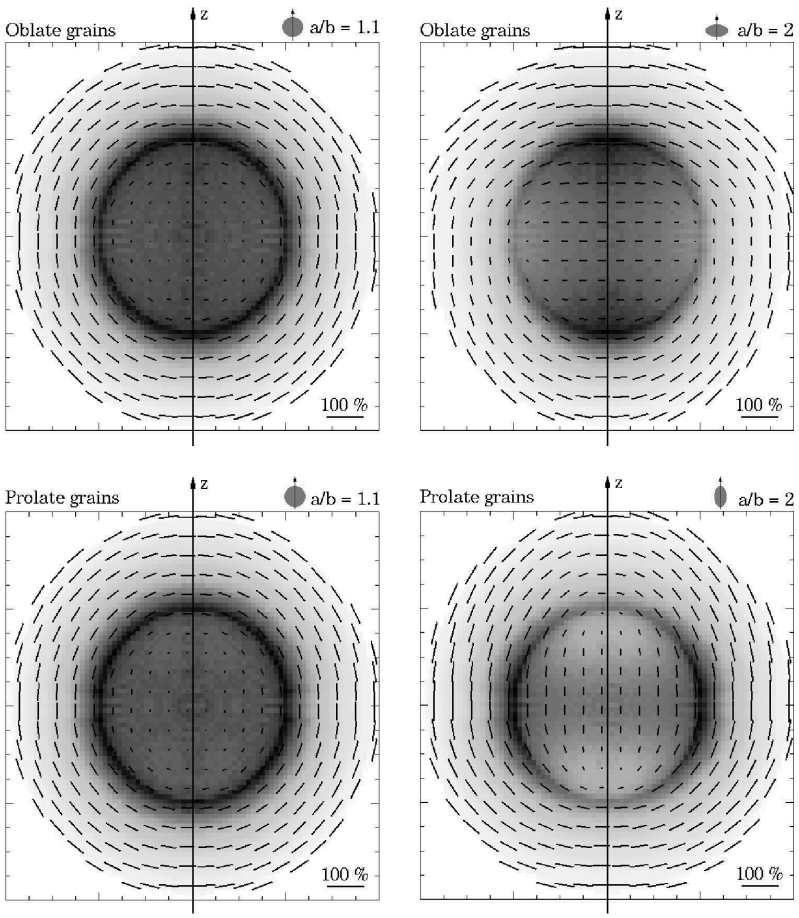

Figure 4. Intensity maps with overlaied polarization pattern of a spherical shell containing perfectly aligned dust grains. While the density distribution was the same in the four simulations, the different shapes of the aligned spheroidal dust grains cause deviations from the centro-symmetric intensity distribution and polarization pattern. *(taken from Wolf et al. 2002[7])*

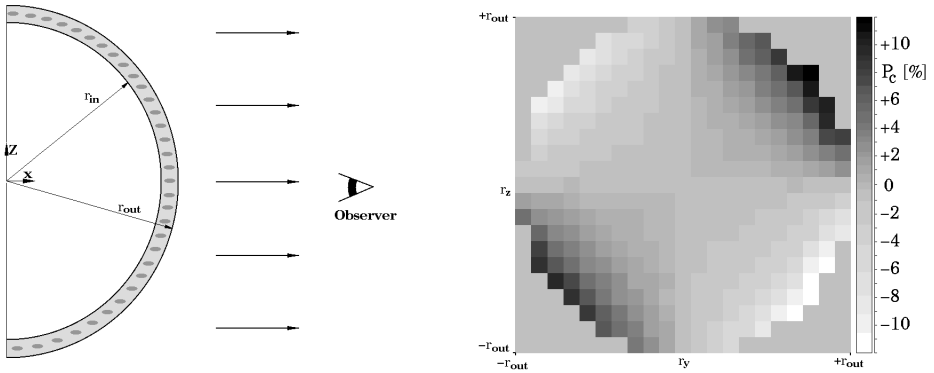

Figure 5. *Left:* Model configuration consisting of a thin dust layer at the surface of a hemisphere. The ratio of the inner radius to the outer one amounts to $r_{\rm in}/r_{\rm out} = 0.99$. The shell contains oblate grains, whereby their rotation axes (b) are oriented parallel to the z-axis. The dark grey oval pattern symbolizes the aligned grains. *Right:* The circular polarization of the scattered radiation arising from this configuration. *(taken from Wolf et al. 2002[7])*

For the estimation of the spatial dust temperature distribution both a concept based on an iterative procedure[14] and a concept based on the immediate correction of the dust grain temperature and the reemission radiation field after absorption of a photon packet are implemented.[16] The main physical processes considered are scattering and absorption by spherical and spheroidal grains† and electrons (Thomson scattering). Further improvements in the efficiency of the estimation of dust temperature distribution[17] and the radiative transfer in optically very thin configurations[15] are considered as well.

It is designed for the simulation of dust temperatures in arbitrary geometric configurations and the resulting observables: spectral energy distributions, wavelength-dependent images, and polarization maps. The main objective is the investigation of "dust-dominated" astrophysical systems such as young stellar objects surrounded by an optically thick circumstellar disk and an optically thin(ner) envelope, debris disks around more evolved stars, asymptotic giant branch stars, the dust component of the interstellar medium, and active galactic nuclei.

ACKNOWLEDGMENTS

This research was supported through the DFG grant Ste 605/10 within the program "Physics of star formation", through the NASA grant NAG5-11645, and through the grant DP.10633 (project 101555).

REFERENCES

1. I. Pascucci, S. Wolf, J. Steinacker, and et al., "The 2D Radiative Transfer Problem: Benchmark Results for Disk Configurations," *A&A, in prep.* , 2002.
2. S. Wolf, *Three-dimensional continuum radiation transfer based on the Monte-Carlo method. Basics and Applications.*, Friedrich Schiller University, Jena, 2001.
3. S. Wolf, F. Gueth, T. Henning, and W. Kley, "Detecting planets in protoplanetary disks: A prospective study," *ApJ* **566**, p. L97, 2002.
4. S. Wolf, O. Fischer, and W. Pfau, "Radiative transfer in the clumpy environment of young stellar objects," *A&A* **340**, p. 103, 1998.
5. S. Wolf, B. Stecklum, and T. Henning, "Pre-main sequence binaries with aligned disks?," in *The Formation of Binary Stars, IAU Symposium No. 200*, B. Reipurth and H. Zinnecker, eds., *ASP Conf. Ser.*, p. 295, 2001.
6. S. Wolf and T. Henning, "AGN polarization models," *A&A* **341**, p. 675, 1999.
7. S. Wolf, N. Voshchinnikov, and T. Henning, "Pre-main sequence binaries with aligned disks ?," *A&A* **385**, p. 365, 2002.
8. S. Wolf, "Inverse Raytracing based on the Monte-Carlo Method," *A&A* **379**, p. 2001, 607.
9. K. Wood, M. Wolff, J. Bjorkman, and B. Whitney, "The Spectral Energy Distribution of HH 30 IRS: Constraining the Circumstellar Dust Size Distribution," *ApJ* **564**, p. 887, 2002.
10. A. Cotera, B. Whitney, and E. Young, "High-Resolution Near-Infrared Images and Models of the Circumstellar Disk in HH 30," *ApJ* **556**, p. 958, 2001.
11. O. Fischer, T. Henning, and H. Yorke, "Simulation of polarization maps. II. The circumstellar environment of pre-main sequence objects.," *A&A* **308**, p. 863, 1996.
12. S. Wolf and T. Henning, "Accelerated Self-Consistent Radiative Transfer based on the Monte-Carlo Method," *Comp. Phys. Comm.* **132**, p. 166, 2000.
13. S. Wolf, "MC3D - 3D Continuum Radiative Transfer, Version 2," *Comp. Phys. Comm.* **in press**, 2002.
14. S. Wolf, T. Henning, and B. Stecklum, "Multidimensional Self-Consistent Radiative Transfer Simulations based on the Monte-Carlo Method," *A&A* **439**, p. 839, 1999.
15. E. Cashwell and C. Everett, *A practical manual on the Monte Carlo Method for random walk problems.*, Pergamon, New York, 1959.
16. J. Bjorkman and K. Wood, "Radiative Equilibrium and Temperature Correction in Monte Carlo Radiation Transfer," *ApJ* **554**, p. 615, 2001.
17. L. Lucy, "Computing radiative equilibria with Monte Carlo techniques," *A&A* **344**, p. 282, 1999.

†Not in the public version - please, contact the author.

18. O. Fischer, *Modellierung der Polarisation in zirkumstellaren Staubhüllen unter Anwendung der Monte-Carlo-Methode, PhD thesis*, Friedrich Schiller University, Jena, 1993.
19. C. Bohren and D. Huffman, *Absorption and scattering of light by small particles*, John Wiley & Sons, New York, 1983.
20. A. Elvius and J. Hall, "Observations of polarization and color in the nebulosity associated with the Pleiades cluster," *Lowell Obs. Bull.* **7**, p. 17, 1967.
21. R. Hajjar and P. Bastien, "Polarimetry of the Interstellar Medium," in *Imaging Polarimetry of Young Stellar Objects*, W. Roberge and D. Whittet, eds., *ASP Conf. Ser.* **97**, p. 355, 1996.
22. J. Kastner and D. Weintraub, "Polarimetry of the Interstellar Medium," in *Dust Envelopes of Evolved Stars: Lessons Learned from Near-Infrared Polarimetric Coronagraphic imaging*, W. Roberge and D. Whittet, eds., *ASP Conf. Ser.* **97**, p. 212, 1996.
23. A. Dollfus and J.-L. Suchail, "Polarimetry of grains in the coma of P/Halley. I - Observations," *A&A* **187**, p. 669, 1987.
24. J. Johnson and T. Jones, "Irradiation effects in a comet's outer layers," *AJ* **101**, p. 1735, 1991.
25. A. Chrysostomou, T. Gledhill, and F. M. et al., "Polarimetry of young stellar objects - III. Circular polarimetry of OMC-1," *MNRAS* **312**, p. 103, 2000.
26. N. Voshchinnikov, "Optical properties of spheroidal dust grains - Forward scattered radiation," *SvA* **34**, p. 535, 1990.
27. S. Kim and P. Martin, "The size distribution of interstellar dust particles as determined from polarization: Spheroids," *ApJ* **444**, p. 293, 1995.
28. T. Onaka, "Polarization of thermal emission from aligned dust grains under an anisotropic radiation field," *ApJ* **553**, p. 298, 2000.
29. N. Voshchinnikov and V. Farafonov, "Optical properties of spheroidal particles," *Ap&SS* **204**, p. 19, 1993.